Title: Nucleoporin NUP210L and BAF-paralogue BAF-L together ensure microtubule organization and nuclear integrity in spermatids

Running Title: NUP210L and BAF-L in spermatids

Maha Al Dala Ali[1, 2], Guy Longepied[1], Nicolas Lévy[1*], Catherine Metzler-Guillemain[1,3], Michael J Mitchell[1].

[1]Aix Marseille Univ, Inserm, MMG, U1251, Marseille, France.

[2] Al-Iraqia University, College of Medicine, Department of physiology, Baghdad, Iraq.

[3]AP-HM, Pôle Femmes-Parents-Enfants, Centre Clinico-biologique AMP-CECOS, Marseille Cedex 5, France.

*Present address: Servier, Research and Development, rue Francis Perrin, 91190 Gif-sur-Yvette.

Correspondence should be addressed to M J Mitchell; Email: michael.mitchell@univ-amu.fr.

Keywords: spermiogenesis – nuclear pore complex – barrier-to-autointegration factor - microtubule – digenic inheritance – male fertility

Summary: Nucleoporin NUP210L and BAF-paralogue BAF-L function redundantly during mouse spermatid nuclear remodeling to concentrate nuclear pores to the flagellar pole, organize the manchette cytoskeleton and prevent nuclear invagination by microtubules.

Abstract

During spermiogenesis, haploid round spermatids differentiate into spermatozoa. This involves nuclear elongation, chromatin compaction, cytoplasm reduction, and formation of the acrosome and the flagellum. These events are orchestrated by cytoskeletal elements - acroplaxome and manchette - that attach to the nuclear envelope (NE) except at the caudal pole where the nuclear pore complexes (NPCs) shift to form a dense array. Here, we use a genetic dissection approach

to reveal function at the caudal NE, through the study of two spermatid-specific proteins, whose human orthologues persist there as spermatids elongate: NUP210L, a transmembrane nucleoporin and BAF-L, paralogue and interactor of chromatin protein BAF. In mice, inactivation of either BAF-L or NUP210L has no impact on fertility. However, we show here that in mice lacking NUP210L, two copies of BAF-L become essential for fertility; in *Nup210l*$^{-/-}$,*Banf2*$^{+/-}$ or *Nup210l*$^{-/-}$,*Banf2*$^{-/-}$ mice, most spermatids arrest during nuclear elongation (step 10-11) with mislocalized NPCs and disorganized manchette microtubules that frequently invaginate the nucleus from the caudal pole. Our results suggest that the NPC array, and BAF-L/BAF, ensure nuclear integrity at the caudal pole during spermatid remodeling.

Introduction

Spermiogenesis is the post-meiotic phase of spermatogenesis when haploid round spermatids transform into specialized motile spermatozoa able to transport the paternal genetic information into the oocyte cytoplasm and create the zygote. To accomplish this, spermatids develop a flagellum for motility and an acrosome to penetrate the oocyte's protective *zona pellucida* layer. To aid motility, and protect the DNA from damage, the nucleus is elongated and condensed. Nuclear compaction involves re-packaging of the chromatin into a dense inactive form by the replacement of almost all histones with small basic proteins, the protamines.

This unique nuclear metamorphosis is structured by cytoskeletal scaffolding that all but surrounds the nucleus (Kierszenbaum and Tres, 2004): the acroplaxome under the acrosome, which is bounded by the perinuclear ring from which descends the manchette, a sleeve of microtubules attached to the lateral nuclear membranes by links involving heterodimers of SUN3 and SUN4 inner nuclear membrane proteins (Calvi *et al.*, 2015; Gao *et al.*, 2020; Pasch *et al.*, 2015). In the mouse, the manchette forms in round spermatids at step 8, just prior to the beginning of elongation, and disappears after both elongation and condensation of the nucleus have occurred at step 13-14 (Lehti and Sironen, 2016). The acroplaxome-acrosome attachment to the nucleus is dependent on the inner nuclear membrane protein DPY19L2 (Pierre *et al.*, 2012). In mice lacking SUN3, SUN4 or DPY19L2 the manchette does not attach to the nucleus and all spermatozoa have compacted round heads, showing that nuclear attachment of the acroplaxome and the manchette are required for nuclear elongation and shaping but not compaction (Calvi *et al.*, 2015; Gao *et al.*, 2020; Pasch *et al.*, 2015; Pierre *et al.*, 2012).

In mouse and human, major changes occur to the NE during spermatid elongation with the dismantling and removal of the nuclear lamina ahead of the spreading acroplaxome (Alsheimer *et al.*, 1998; Schütz *et al.*, 2005; Elkhatib *et al.*, 2015; Ho 2010). When the manchette forms, NPCs move from the lateral NE to the caudal pole of the nucleus and form a tight array there,

but are excluded from the basal plate where the centrioles and the flagellum attach to the nucleus (Dooher and Bennett 1973; Ho 2010). How NPCs shift from under the manchette is unknown, but it could involve SUN1 which moves to the caudal pole at the same time (Göb *et al.*, 2010). *Sun1*-knockout male mice produce no spermatids due to a meiotic block, and so how SUN1 contributes to spermiogenesis has not yet been investigated (Chi *et al.*, 2009; Ding *et al.*, 2007). Since the NPC is the major non-vesicular route in and out of the nucleus, the caudal pole must be a site of intense trafficking across the nuclear membrane during nuclear remodelling. Nevertheless, in contrast to the rest of the spermatid NE, little else is known about organisation and function within the zones of cytoplasm, NE or nucleoplasm that juxtapose the nuclear attachment site of the flagellum.

Evidence that the NPC plays an important role in spermatid nuclear compaction and remodelling has recently emerged from a genetic study of human male infertility. A biallelic loss-of-function (LoF) mutation in the gene encoding NUP210L, a spermatid-predominant paralogue of the transmembrane nucleoporin NUP210, was identified in an infertile man with a unique phenotype characterized by spermatozoa with a large uncompacted head and histonylated chromatin (Arafah *et al.*, 2021). We have shown that NUP210L localizes to the caudal nuclear pole of elongating spermatids and spermatozoa, in mouse and human (Al Dala Ali *et al.*, 2024). Its paralogue NUP210 is thought to form an octamer ring around the nuclear pore membrane, that may optimize nuclear pore channel function by buffering it from external forces within the NE (Zhang *et al.*, 2020). The inactivation of *Nup210l* alone in the mouse does not, however, impact fertility or chromatin condensation, although spermatozoa do show morphological changes in the head and flagella, and reduced numbers are motile (Al Dala Ali *et al.*, 2024). Thus, whether NUP210L is essential for nuclear remodeling and chromatin condensation during human spermiogenesis remains an open question.

50 We have previously shown that, in human spermatids, the small conserved chromatin protein
51 BAF, and its spermatid-predominant paralogue BAF-L, shift from the nucleoplasm to the
52 caudal nuclear pole as nuclear elongation begins, suggesting that they contribute to nuclear
53 remodelling (Elkhatib *et al.*, 2017). In somatic cells, BAF exists as homodimers that when
54 dephosphorylated can bind non-specifically to double stranded DNA, promoting bridging and
55 compaction of DNA (Skoko *et al.*, 2009; Zheng *et al.*, 2000). In somatic cells, BAF-DNA
56 interactions are at the root of fundamental cellular processes such as nuclear membrane
57 reassembly at the end of mitosis, NE repair, gene regulation, the innate immune response to
58 cytosolic DNA and the DNA damage response (Sears and Roux, 2020). In contrast to BAF,
59 little is known about BAF-L function except that it is unable to bind DNA, can form
60 heterodimers with BAF and has reduced affinity for the LEM-domains bound by BAF (Tifft *et*
61 *al.*, 2006). It has been proposed that BAF-L may regulate BAF function in spermatids but three
62 independent studies, plus the present study, find that males lacking BAF-L are fertile, (Niu *et*
63 *al.*, 2021; Huang *et al.*, 2022; Lu *et al.*, 2019) providing no insights into the role of BAF-L.
64 Here we present mice carrying null alleles for both BAF-L and NUP210L. We created these
65 mice to look for functional interactions between BAF-L and NUP210L, based on their co-
66 localisation at the caudal pole in human elongating spermatids (Elkhatib *et al.*, 2017; Al Dala
67 Ali *et al.*, 2024). In stark contrast to the fertility of the single knockouts of BAF-L or NUP210L,
68 we find that male mice lacking NUP210L are sensitive to haploinsufficiency for BAF-L; males
69 are infertile, have a striking deregulation of microtubule organisation during nuclear elongation
70 and produce only low numbers of immotile spermatozoa, most with abnormal but compacted
71 heads. Our study shows that, in spermatids, BAF-L and NUP210L are mutually redundant
72 components of an important nexus between the chromatin, the NPC and the cytoskeleton,
73 bringing function at the caudal nuclear pole of the elongating spermatid into sharp focus.
74 **Results**

75 **Normal fertility and testicular histology in mice lacking BAF-L**

76 To investigate the biological function of BAF-L in vivo, we used CRISPR-Cas9 technology to
77 target its coding gene, *Banf2,* and created a mouse line carrying the null allele, *Banf2*^{em42Mmjm},
78 hereafter referred to as *Banf2*$^{-}$. The *Banf2*$^{-}$ allele has a 23 base pair (bp) deletion in exon 3 that
79 includes the initiation codon (based on transcript NM_1178477.5 - Fig. S1A). Purification and
80 sequencing of RT-PCR products from wild type and *Banf2*$^{-/-}$ adult testis revealed that the 23 bp
81 deletion induces the skipping of exon 3 that encodes the N-terminal half of BAF-L (42 of 90
82 amino acids) (Fig. S1B). In exon 4, there is one in-frame ATG at codon 53 but it is in a weak
83 Kozak context, ctgATGc, indicating that no part of BAF-L is expressed from our *Banf2*$^{-}$ allele.
84 As in previously published reports of *Banf2*-KO mice (Huang *et al.*, 2022; Lu *et al.*, 2019; Niu
85 *et al.*, 2021), our *Banf2*$^{-/-}$ male mice are fertile. We found them to have normal litter frequency
86 and litter size (Fig. S2A). Testis size and weight were normal (Fig. S2C) No histological
87 anomalies of spermatogenesis were evident (Fig. S2D), and spermatozoa had normal
88 morphology, count and motility (Fig. S2E, F and G).

89 **Two copies of *Banf2* are required for male fertility in mice lacking *Nup210l***

90 Nuclear pore complexes reorganize into a tight array at the caudal nuclear pole, as the manchette
91 forms and spermatid elongation initiates, and we have shown that this is also the case for BAF,
92 BAF-L, the spermatid-specific nucleoporin NUP210L and the widely expressed nucleoporin
93 NUP153 (Al Dala Ali *et al.*, 2024; Elkhatib *et al.*, 2017), indicating functional coordination,
94 although mice lacking either BAF-L or NUP210L are fertile. As part of an effort to identify
95 function at the spermatid posterior pole, we generated mice carrying null alleles for both *Banf2*
96 and *Nup210l.*

97 We first tested the fertility of mice carrying three combinations of null alleles for
98 *Nup210l* and *Banf2* (*Banf2*$^{-/-}$, *Nup210l*$^{+/-}$; *Banf2*$^{+/-}$,*Nup210l*$^{-/-}$; *Banf2*$^{-/-}$,*Nup210l*$^{-/-}$). Five males
99 of each genotype and 3 double heterozygote male controls (*Banf2*$^{+/-}$;*Nup210l*$^{+/-}$) were paired

100 with two WT females over a period of two months. The average litter size for each genotype is
101 shown in Table 1.

Genotype		Fertile males/Total males	Litter size (mean ± SEM)
Banf2	*Nup210l*		
+/-	+/-	3/3	12.0 ± 1
-/-	+/-	5/5	11.7 ± 0.6
+/-	-/-	0/5	0
-/-	-/-	0/5	0

102 **Table 1**: Fertility test of *Banf2,Nup210l* mutant males.

103 Mice with zero copies of wild-type *Nup210l* and one or zero copies of wild-type *Banf2* were
104 infertile (Table 1). Thus, in mice lacking NUP210L function, male fertility is sensitive to
105 reduced expression of BAF-L, while in mice with reduced expression of BAF-L, NUP210L
106 function is critical for fertility.

107 **Lack of BAF-L and NUP210L affect sperm morphology and concentration**

108 We next investigated the nature and the cause of the infertility in *Banf2*$^{+/-}$,*Nup210l*$^{-/-}$ and *Banf2*$^{-}$
109 $^{/-}$,*Nup210l*$^{-/-}$ males, through the analysis of testicular and epididymal histology, and epididymal
110 spermatozoa. Testis weight in adult infertile mutants (2 months old) was not significantly
111 different to that of the control group (Fig. 1A, 1C). However, spermatogenic activity was clearly
112 disrupted in infertile double mutant males, as evidenced by abnormally low numbers or
113 complete absence of spermatozoa in the epididymis (Fig. 1B).

114 To assess the quality of sperm production, epididymal sperm samples were collected from 16
115 double mutant males of the *Banf2*$^{+/-}$,*Nup210l*$^{-/-}$ or *Banf2*$^{-/-}$,*Nup210l*$^{-/-}$ genotype. Compared to
116 control littermates (n=7) the sperm count was significantly lower in the double mutants (Fig
117 1D): five had less than 30%, nine less than 10%, and two had no spermatozoa. Furthermore,
118 98% of the sperm in the mutant mice were immotile (Fig. 1E). Morphological examination
119 revealed that 90% of sperm have an abnormal head shape, with 76% losing their hook-like
120 characteristic shape, and 14% exhibiting a large uncompacted head (Fig. 1F). Additionally, we
121 observed tail abnormalities characterized by midpiece defects (Fig. 1F). These findings show

122 that reduced expression of BAF-L in the absence of NUP210L impacts spermatozoa production
123 and morphogenesis.

124 **Spermatids arrest during elongation in *Nup210l*$^{-/-}$ mice carrying a *Banf2* null allele.**

125 Histological analysis of testes stained with hematoxylin and Periodic Acid-Schiff (H-PAS)
126 showed that meiosis and spermatid development were normal up to step 10 of spermiogenesis.
127 In contrast, the number of elongated spermatids at later steps was greatly reduced in
128 *Banf2*$^{+/-}$,*Nup210l*$^{-/-}$ and *Banf2*$^{-/-}$,*Nup210l*$^{-/-}$ males (Fig.S2). This was most evident in stage I-
129 VIII tubules, where condensed elongated spermatids are normally abundant (Fig. 2A). Using
130 the TUNEL assay, in three biological triplicates, we found a 30-fold increase in apoptotic cells
131 in the seminiferous tubules of *Banf2*$^{-/-}$,*Nup210l*$^{-/-}$ versus control males (185 ± 12 per 20 tubules
132 versus 6 ± 1 per 20 tubules, Fig. 2B, 2C). Most apoptotic cells were uncondensed elongated
133 spermatids, identified by both their morphology and their location within seminiferous tubules
134 (Fig. 2B). Our results suggest that, in *Banf2*$^{+/-}$,*Nup210l*$^{-/-}$ and *Banf2*$^{-/-}$,*Nup210l*$^{-/-}$ males, the
135 majority of spermatids fail to progress beyond early elongation steps, show no signs of nuclear
136 condensation and are eliminated by apoptosis prior to step 13.

137 **Inefficient chromatin remodeling in infertile double mutant mice**

138 To investigate whether histone-to-protamine replacement is affected in *Banf2*$^{+/-}$,*Nup210l*$^{-/-}$ and
139 *Banf2*$^{-/-}$,*Nup210l*$^{-/-}$ males, we initially determined chromomycin A3 (CMA3) staining of
140 epididymal spermatozoa. CMA3 is a fluorochrome specific for guanine-cytosine (GC)-rich
141 sequences in histonylated chromatin, but its binding is blocked when the chromatin is packaged
142 with protamines. Normal spermatozoa exhibit a negative CMA3 test result, and a positive result
143 indicates histone retention and protamine deficiency. In both *Banf2*$^{+/-}$,*Nup210l*$^{-/-}$ and *Banf2*$^{-}$
144 $^{/-}$,*Nup210l*$^{-/-}$ males, we observed that approximately 22-25% of the sperm were CMA3 positive
145 compared to only 1% in controls (Fig. 3 A and B).

146 We then assessed histone H4 acetylation by immunofluorescence. The timing and progression
147 of H4 acetylation in the mutant animals appeared normal, beginning at spermatid step 8 and
148 intensifying at step 9 and 10, before receding to the caudal pole at step 11 and 12 and
149 disappearing in later stages (Fig.3 C). Although the pattern of acetylated histone 4 signal
150 appears normal up to the block, the presence of significant number of CMA3 positive cells in
151 the epididymis of double mutants indicates that the histone-to-protamine replacement is
152 perturbed in some but not all spermatids.

153 **Loss of NE integrity in round spermatids of *Banf2*$^{-/-}$,*Nup210l*$^{-/-}$ males**

154 To investigate the form of the NE and the evolution of the nuclear lamina (NL) in round
155 spermatids in *Banf2*$^{-/-}$,*Nup210l*$^{-/-}$ males, we used an antibody against lamin B1. In controls and
156 double-KO mice, we observed the normal pattern of labelling (Pierre *et al.*, 2012), with lamin
157 B1 at the nuclear periphery, except under the developing acrosome in round spermatids until
158 its disappearance at the initiation of nuclear elongation, indicating that the absence of BAF-L
159 and NUP210L does not affect the dismantling of the NL in round spermatids. Nevertheless,
160 these analyses revealed a major difference in the shape of the round spermatid nucleus: in
161 controls it was round, but in *Banf2*$^{-/-}$,*Nup210l*$^{-/-}$ males, beginning at step 1, it was deformed,
162 appearing elliptical, angular or indented (Fig. 4A). No differences were obvious later in step 9-
163 10 spermatids, with both control and *Banf2*$^{-/-}$,*Nup210l*$^{-/-}$ showing uniform elongated nuclei.
164 These observations indicate that BAF-L and NUP210L are required to maintain a spherical NE
165 in round spermatids. Interestingly, we did not observe deformity of the NE in disaggregated
166 spermatids (Fig. S4), implying that, in the testis, round spermatid nuclei lacking BAF-L and
167 NUP210L are being deformed by extracellular forces exerted from within the seminiferous
168 epithelium.

169 **BAF shows increased nuclear retention in *Banf2*$^{-/-}$,*Nup210l*$^{-/-}$ round spermatids**

170 Since BAF-L can heterodimerize with BAF *in vitro*, we investigated how the absence of BAF-
171 L affected BAF localisation in *Banf2*$^{-/-}$,*Nup210l*$^{-/-}$ spermatids by immunofluorescence. In
172 control mice, BAF exhibits cytoplasmic and nucleoplasmic localization in step 1-3 round
173 spermatids. BAF becomes exclusively nucleoplasmic in spermatids from step 4-5, concentrated
174 at a point on the nuclear periphery at the posterior pole, where the distal centriole and the
175 flagellar axoneme contact the nucleus. In step 9 elongated spermatids, it is only present at the
176 caudal pole next to the flagellum attachment site. BAF is not detected in spermatids after step
177 9 (Fig. 4B). In epididymal sperm, there is a complete absence of BAF signal (Fig. S4).
178 In *Banf2*$^{-/-}$,*Nup210l*$^{-/-}$ males, unlike controls, BAF predominates in the nucleus in step1-3 round
179 spermatids (Fig. 4B). The specific localisation of BAF at the caudal pole in step 9 spermatids
180 is as in controls, but unlike in controls, BAF persists at the caudal pole in later elongating
181 spermatids (Fig. 4B) and is still present in 23% of epididymal spermatozoa (n=100) (Fig. S4).
182 **Nuclear pore array disorganised at the caudal pole in *Banf2*$^{-/-}$,*Nup210l*$^{-/-}$ spermatids**
183 NUP210L is thought to be a component of the NPC in spermatids. We therefore next
184 investigated the localization of the NPC in *Banf2*$^{-/-}$,*Nup210l*$^{-/-}$ spermatids using an antibody
185 against NUP153, a component of the NPC present in spermatids. Normally, the NPC is located
186 at the posterior nuclear pole surrounding the basal plate where the flagellum connects to the
187 nucleus. In control spermatids, NUP153 is detected along the caudal limit of the nucleus distal
188 to the acrosome. However, in the *Banf2*$^{-/-}$,*Nup210l*$^{-/-}$ males, we observed altered NPC
189 localization in elongating spermatids, where the NUP153 signal was either concentrated at the
190 ventral part of the caudal pole or completely displaced from the posterior nuclear pole (Fig. 4C).
191 **Inefficient organization of manchette microtubules in *Banf2*$^{-/-}$,*Nup210l*$^{-/-}$ spermatids**
192 Using transmission electron microscopy (TEM) of testis sections, we observed abnormal
193 nuclear development in elongating spermatids in both *Banf2*$^{+/-}$,*Nup210l*$^{-/-}$ and *Banf2*$^{-/-}$,*Nup210l*$^{-}$
194 $^{/-}$ males when compared to controls. The most striking anomaly in the double mutant was deep

195 invagination of the NE from the caudal pole, visible in approximately 30% of sections (Fig. 5
196 B, C, D). In cross-sections of uncondensed spermatid nuclei, the invaginated NE appears to be
197 intact and to surround ectopic microtubules (Fig. 5F), but normally positioned manchette
198 microtubules could also be observed parallel to the sectioned NE (Fig. 5H). Nuclear pores were
199 never seen on the invaginated NE. Nuclear pores showed a more restricted localisation at the
200 caudal nuclear pole of uncondensed elongating nuclei in *Banf2*$^{-/-}$,*Nup210l*$^{-/-}$ males, and appeared
201 to be only on one side of the nuclear invagination (Fig. 5G, H) confirming our observations
202 with immunofluorescent localization of NUP153 (Fig 4C). In compacted spermatid nuclei,
203 ectopic microtubules were not evident but nuclear invaginations remained, appearing as large
204 vacuoles (Fig. 5J, K, L).
205 Further analysis using immunofluorescence with an antibody against acetylated alpha tubulin
206 (Ac-α-tubulin) revealed defective manchette formation in about 45% of *Banf2*$^{-/-}$,*Nup210l*$^{-/-}$
207 spermatids (Fig. 5M). Defective manchettes, never observed in controls, were characterized by
208 discontinuities in the microtubule sleeve, possibly a consequence of microtubule bundles being
209 diverted from the manchette through a failure to prevent their invagination of the nucleus at its
210 caudal pole.

211 **Discussion**

212 Our study provides clear evidence that BAF-L and NUP210L are functionally connected genes
213 required for efficient nuclear remodelling in spermatids, and male fertility. Lack of either BAF-
214 L or NUP210L in the mouse is compatible with full fertility (Lu *et al.*, 2019; Niu *et al.*, 2021;
215 Al Dala Ali *et al.*, 2024) although in the case of NUP210L loss there is a drop in spermatozoa
216 quality with half being immotile (Al Dala Ali *et al.*, 2024). Here, however, we show that in
217 mice lacking NUP210L, nuclear morphology in round spermatids and manchette formation
218 become sensitive to BAF-L dose, establishing that BAF-L and NUP210L play mutually
219 redundant roles required to maintain the structural integrity of the round spermatid nucleus, to

array the NPCs at the caudal pole and to organise microtubules into the manchette. The consequence of insufficient BAF-L in the absence of NUP210L is a catastrophic failure of spermatid nuclear remodelling, leading to male infertility. We reveal function at the caudal NE in spermatids, previously hidden by the functional redundancy of BAF-L and NUP210L.

Although it has been known for over 50 years that NPCs shift to a tight array at the caudal nuclear pole as the manchette forms and spermatid elongation begins (Dooher and Bennett 1973), there has been little notion of how the NPC contributes to spermatid differentiation, beyond controlling traffic into and out of the nucleus. Our study reveals that one of the roles of the NPC array, is to ensure nuclear integrity by regulating the position of polymerising manchette MTs relative to the nucleus. It is not clear how NUP210L and BAF-L attain this, but a similar phenotype of microtubule invagination of the spermatid nucleus from its caudal pole has been reported in rats treated with taxol (Russell *et al.*, 1991), and in neurons where the normally axonal tau protein is ectopically positioned close to the nucleus in the cell body (Paonessa *et al.*, 2019). Since both taxol and tau stabilise microtubules, the NPC array may normally block stabilisation of MTs that contact the caudal nuclear pole, during the formation of the manchette in step 8 spermatids. This might serve to guide the proto-manchette MTs to the SUN3/SUN4 links in the lateral NE and on to join the sub-acrosomal perinuclear ring (Calvi *et al.*, 2015; Gao *et al.*, 2020; Pasch *et al.*, 2015). Our results show that the spermatid NPC array is an integral part of spermatid NE compartmentalisation, protecting the caudal NE from invagination by MTs as they polymerise to form the manchette. It may achieve this by preventing the diffusion of SUN3/SUN4 MT-tethering links from the lateral NE.

The structural organisation and function of NUP210L has not been studied directly, and can only be inferred from what is known about its paralogue NUP210. NUP210 forms an elastic octamer ring that encircles the nuclear pore membrane where it is proposed to buffer pore function, control pore spacing, and recruit transcription factors to chromatin at the NPC (Zhang

245 *et al.*, 2020; Cohen *et al.*, 2003; Raices *et al.*, 2017). In breast cancer cells, through an
246 interaction with the LINC complex protein SUN2, NUP210 is part of a mechanosensitive
247 connection between the chromatin and the cytoskeleton that is important for metastasis (Amin
248 *et al.*, 2021). SUN2 is not present in spermatids, but its close paralogue SUN1, with which it is
249 partially redundant, has been localised to the caudal pole in elongating spermatids along with
250 nesprin-3, a LINC complex partner of SUN1 and SUN2 (Göb *et al.*, 2010), and so could link
251 NUP210L to the cytoskeleton. Although mice lacking nesprin-3 are fully fertile, the study of
252 mice lacking nesprin-3 and BAF-L or nesprin-3 and NUP210L should allow this hypothesis to
253 be tested. Thus, in spermatids, NUP210L could have a physical effect on the arrangement of
254 NPCs and their core function, be part of a mechanosensitive chromatin-cytoskeletal link and
255 regulate gene expression. In *Banf2*$^{-/-}$,*Nup210l*$^{-/-}$ round and elongating spermatids, the weakening
256 of nuclear integrity could therefore be a result of the NPC decoupling from both a SUN1-
257 nesprin-3 LINC complex and a chromatin-BAF/BAF-L-cytoskeleton link.
258 Given that BAF-L can form heterodimers with its paralogue BAF, a conserved chromatin
259 protein, it is most probable that, in the spermatid nucleus, BAF-L is indirectly bound to specific
260 sites on the chromatin through BAF (Tifft *et al.*, 2006). The binding of BAF/BAF-L
261 heterodimers (WT fertile mice) or BAF homodimers (*Banf2*-KO fertile mice) to DNA may
262 enable the resulting chromatin to link to the cytoskeleton through the NPC. Nevertheless, how
263 BAF or BAF-L connect to the NPC or the NE in spermatids is not clear. Most of the proteins
264 known to link BAF to the NE in somatic cells were not detected in human or rodent spermatids
265 (lamin A/C, emerin, LEMD3, LEMD2), or do not localise to the caudal pole (Vester *et al.*, 1993;
266 Elkhatib *et al.*, 2017; Elkhatib *et al.*, 2015). A candidate protein that might interact with BAF-
267 L, is the spermatid-predominant protein, LEMD1, that has an N-terminal LEM-domain and a
268 C-terminal transmembrane domain. In human, LEMD1 labels the nucleoplasm in round
269 spermatids, shifting to the caudal pole as the spermatid elongates (Elkhatib *et al.*, 2017). As a

270 possible explanation for the observed functional redundancy of NUP210L and BAF-L in
271 maintaining spermatid nuclear integrity, we propose that the NPC normally participates in two
272 distinct chromatin-cytoskeleton links: the first involving NUP210L, SUN1-nesprin-3 and
273 possibly BAF, and the second a nucleoporin other than NUP210L and BAF-L.
274 In human, the infertile man lacking NUP210L has severe oligozoospermia and produced
275 immotile spermatozoa (100%) with large uncondensed heads (83%) and retained histones
276 (100%) (Arafah *et al.*, 2021). The *Banf2*$^{-/-}$,*Nup210l*$^{-/-}$ and the *Banf2*$^{+/-}$,*Nup210l*$^{-/-}$ mice presented
277 here do not reproduce the human sperm phenotype exactly but there are similarities that may
278 indicate common consequences of compromised NPC function during spermiogenesis: severe
279 but incomplete spermatogenic blockage during nuclear remodelling, epididymal spermatozoa
280 with uncondensed heads (14%), histones retained in spermatozoa (25%) and few motile sperm
281 (1-2%). Based on our findings in the mouse, the severity of the human *NUP210L*-KO
282 phenotype indicates that a biological process able to complement the loss of NUP210L function
283 is not active in the patient. This could be the result of a recent genetic mutation (digenism) or
284 an ancient mutation common to all humans. One candidate for the former, carried by the patient,
285 is a rare potentially pathogenic missense variant (p.Pro485Leu) in NUP153, a nucleoporin
286 present at the spermatid caudal nuclear pole (Al Dala Ali *et al.*, 2024).
287 Our double knockout model reveals an example of functional redundancy in a previously
288 unknown biological process indispensable for spermiogenesis. Genetic redundancy has most
289 commonly been evidenced between paralogues, but rarely between unrelated genes, since it is
290 practically impossible to identify genes involved in distinct redundant pathways in the absence
291 of sequence homology. Nevertheless, there are many reports of conserved testis predominant
292 genes whose inactivation in the mouse does not appear to have any effect on fertility in the
293 laboratory environment, indicating that genetic redundancy is common during spermatogenesis
294 (Khan *et al.*, 2018; Miyata *et al.*, 2016; Lu *et al.*, 2019) As is clearly illustrated by our findings,

295 functional redundancy renders biological processes invisible to molecular genetics based on
296 single-gene inactivation. Furthermore a large study of almost 1000 azoospermic men only
297 identified plausible monogenic causes in 20% of their cohort (Nagirnaja *et al.*, 2022). Digenism
298 should therefore be considered when designating candidate causal genetic variants in the
299 context of human male fertility. Firstly, even in an infertile man with an obvious gene
300 inactivation, mutation of an unrelated second gene may underlie the phenotype, and this could
301 confound attempts to validate the variant as causal in the mouse. Secondly when filtering
302 variants from exome sequencing data under a digenic model the allelic frequencies that predict
303 less than 1:10 000 affected individuals are high and would be excluded from monogenic screens:
304 *e.g.,* 1:10 for autosomal recessive mutations in each gene and 1:100 for autosomal dominant or
305 X-linked mutations. Thirdly, in human cases the pathogenic combination of gene variants is
306 already created, limiting possibilities. Identifying the causal variants will of course be arduous
307 at such high allelic frequency cut-offs, requiring mouse models, but should be investigated in
308 best case scenarios involving unambiguous LoF mutations in testis-specific genes. The
309 potential rewards are to uncover biological processes that presently cannot even be imagined.

310 **Material and Methods**

311 **Generation of knockout mice**

312 Knockout alleles in *Banf2* and *Nup210l* were created by non-homologous end-joining repair of
313 a Cas9 generated double strand break as previously described for *Nup210l* (Al Dala Ali *et al.*,
314 2024). The specific guide RNA sequence (+PAM) used to target *Banf2* was
315 CCCATGTCTGTTGCAGAAGA (+TGG). We selected the allele *Banf2*^{em42Mmjm} with a
316 deletion of the first 23 nucleotides from exon 3 - AAGATGGACGACATGTCGCCCAG. The
317 alleles were created in the C57BL/6NCrl strain. Double mutants were created from mice
318 produced by backcrossing to the outbred Swiss strain. The mice presented in this study are on

319 a mixed C57BL/6NCrl-Swiss background. The necessary approval for our study was obtained
320 from our regional animal experimentation ethical committee, CEEA14.

321 **RT-PCR analysis of testis transcripts from the *Banf2*^{em42Mmjm} allele**

322 Transcripts were amplified with primers in exon 1: o5845f -
323 ACCCGCCGTTACAGATCCCAG and exon 4: o5847r – TCAGGCAGGTGGAGCTCTGG.
324 After agarose electrophoresis, the amplified bands were cut from the gel, purified and
325 sequenced with the same primers.

326 **Sperm analysis**

327 For sperm analysis, the cauda epididymis of each mouse was dissected into small pieces using
328 two scalpels to allow motile sperm to swim out. These pieces were then incubated in 2 ml of
329 medium (DMEM, HEPES - 22320022 Thermofisher) at 37°C for 10 minutes. Sperm
330 suspensions were obtained, and the motility of the sperm was assessed by direct microscope
331 observation. The total number of sperm was estimated using a Malassez hemocytometer, and
332 the morphology of the sperm was evaluated after staining with SpermBlue stain (Microptic,
333 Barcelona, Spain), following the standard protocol. The morphology of the head and tail was
334 assessed individually for each mouse, with a minimum count of 100 cells per sample.

335 **Testis and epididymis histology**

336 Mice testes and epididymis were obtained from both control and mutant mice. They were fixed
337 in Bouin's solution at room temperature overnight. The fixed tissues were then dehydrated,
338 embedded in paraffin, and sectioned to a thickness of 7 µm for the testis and 5 µm for the
339 epididymis using an Ultrathin Microtome from Leica, Germany. The testis sections were
340 stained with H-PAS staining (Sigma-Aldrich), while the epididymis sections were stained with
341 Mayer's hematoxylin and eosin from Sigma-Aldrich, following a standard protocol

342 **Immunofluorescence - Testis sections**

343 Testis samples were collected and fixed in 4% paraformaldehyde (PAF) at 4 °C overnight. The
344 fixed testes were dehydrated in a graded sucrose solution, embedded in OCT, and cut into 5 µm
345 sections. The sections were then rehydrated with phosphate-buffered saline (PBS) for 5
346 minutes, permeabilized with 0.3% Triton X-100 in PBS for 30 minutes, and blocked with 1%
347 BSA, 7% NGS, and 0.1% Triton X-100 for 1 hour at room temperature. The sections were
348 incubated overnight with primary antibodies in the blocking solution. After three washes in a
349 0.1% Triton X-100 solution, the slides were incubated with secondary antibodies in the
350 blocking solution for 1 hour at room temperature. Following 3 washes with 0.1% Triton X-100
351 in PBS, the nuclei were counterstained with 100 ng/ml DAPI in PBS, and the slides were
352 mounted using fluoromount-G mounting media (Southern Biotech).

353 **Immunofluorescence - Testis cell spreads**

354 To isolate individual cells, the testes were retrieved, and the tunica albuginea removed. The
355 testicular pulp was dilacerated using two scalpels. The cells obtained were suspended in 7 ml
356 of DMEM, HEPES medium (Thermofisher). They were then washed twice with PBS, fixed in
357 a 2% paraformaldehyde solution for 5 minutes, rinsed twice again with PBS, and finally spread
358 onto slides using a Cytospin (Shandon). The slides were permeabilized with 0.5% Triton X-
359 100 in PBS for 15 minutes and blocked with a solution of 1% BSA and 7% NGS at room
360 temperature for 1 hour. Immunofluorescence was then performed as described above for
361 testicular sections.

362 **Antibodies**

363 The following primary antibodies were used for immunofluorescence investigations at the
364 specified dilution: anti-Lamin B1 (ab151735 - Abcam) 1:100, anti-acetylated histone H4 06866
365 - Upstate) 1:400, and anti-NUP153 (ab24700 - Abcam) 1:50, anti-Ac-α-tubulin (T7451 - Sigma)
366 1:20, and anti-BAF (ab129184 - Abcam) 1:100.

367 Acrosomes were labeled directly with Lectin PNA Alexa Fluor™Plus 594 (L32459 -
368 Thermofisher) 1:600. Secondary antibodies were from ThermoFisher: Goat anti-Rabbit IgG
369 Alexa Fluor™Plus 488 (A32731) 1:400; Goat anti-Mouse IgG Alexa Fluor™Plus 488 (A11001)
370 1:400. Donkey anti-Rabbit IgG Alexa Fluor™ Plus 647 (Invitrogen-A32795) IF-1:400

371 **Terminal deoxynucleotidyl transferase dUTP nick-end labeling (TUNEL) assay on testes**

372 The testes were collected and fixed with 4% PAF at 4°C overnight, dehydrated, and embedded
373 in paraffin. They were then sectioned to a thickness of 5 μm using a microtome. The resulting
374 slides were heated at 55°C for 30 minutes, followed by deparaffinization and rehydration.
375 Subsequently, the slides were incubated with a freshly prepared solution containing 0.1% Triton
376 and 0.1% sodium citrate for 20 minutes at 37°C. After two rinses with PBS, the slides were
377 incubated with a blocking solution (3% BSA, 10% NGS in 10mM Tris-HCl, pH 7.6) for 45
378 minutes at room temperature. Following this, the slides were incubated with a Tunnel mixture
379 (*In Situ* cell detection kit, Roche) for 1 hour at 37°C. After three washes with PBS, the nuclei
380 were stained with a solution of 100 ng/ml DAPI in PBS and mounted using Fluoromount-G
381 mounting media (Southern Biotech).

382 **Chromomycin A3 staining**

383 The sperm was washed twice with PBS, then fixed in a mixture of methanol and acetic acid
384 (3:1 v/v) for 30 minutes at 4°C. The sperm was spread onto slides and allowed to air-dry. Each
385 slide was stained by applying a solution of chromomycin A3 (0.25 mg/ml) in McIlvain buffer
386 at pH 7.0 for 20 minutes. Afterward, the slides were rinsed twice in McIlvain buffer. The nuclei
387 of the sperm were counterstained with a solution of Hoechst (0.5 g/ml) for 5 minutes and rinsed
388 twice with PBS. Fluoromount-G mounting media was used for mounting the slides. Slides were
389 examined using a fluorescence microscope (ApoTome2, Germany).

390 **Transmission electronic microscopy**

391 The testes were fixed overnight at 4°C using a solution of 2.5% glutaraldehyde and 2% PFA in
392 0.1M sodium cacodylate buffer. The following day, the testes were washed three times in
393 sodium cacodylate buffer for 10 minutes each and then post-fixed in 2% osmium tetroxide in
394 0.1M cacodylate buffer for 1 hour at room temperature. After the post-fixation, the testes were
395 washed three times in buffer for 15 minutes each and dehydrated in a series of ethanol
396 concentrations (25%, 50%, 75%, and 100%). Subsequently, the testes were embedded in epoxy
397 resins. Ultrathin sections of 70 nm thickness were obtained using a Leica UC7 instrument and
398 deposited on slot grids. These sections were contrasted with 1% aqueous uranyl acetate for 10
399 minutes and lead citrate for 4 minutes. The resulting grids were observed using an FEI Tecnai
400 G2 microscope operating at 200 KeV, and the acquisition of images was performed using a
401 Veleta camera from Olympus, Japan.

402 **Statistical Analysis**

403 The significance of the variance between the means in study groups was assessed using
404 Student's t-test. A *p*-value below 0.05 was considered significant.

405

406 **Acknowledgements:** We thank Nicolas Brouilly and Aïsha Aouane for help with electron
407 microscopy analyses performed at PiCSL-FBI core facilty (IBDM, AMU-Marseille), member
408 of the France-BioImaging national research infrastructure. We are very grateful to Stéphane
409 Zaffran, Gaëlle Odelin and Adeline Spiga-Ghata of the MMG Animal House Facility for
410 enabling our mouse work. We also thank Keltouma Ali Nehari and Paul Picot for attentive
411 animal care.

412 **Competing Interests:** No competing interests declared.

413 **Funding:** M.A.-D.-A. was supported by funding from the Iraqi Ministry of Higher Education
414 and Scientific Research, and from the MarMaRa Institute. The project was supported by
415 funding from the Agence de la Biomédecine, under the call "PMA, Médecine Fœtale et

Diagnostic Génétique" (2017-56). Funding was also received from Inserm and Aix Marseille University, and from the French government under the France 2030 investment plan, as part of the Initiative d'Excellence d'Aix-Marseille Université - A*MIDEX (AMX-19-IET-007).

Data availability: All relevant data can be found within the article and its supplementary information.

References

Al Dala Ali, M., Longepied, G., Nicolet, A., Metzler-Guillemain, C. and Mitchell, M. J. (2024). Spermatozoa in mice lacking the nucleoporin NUP210L show defects in head shape and motility but not in nuclear compaction or histone replacement. *Clin. Genet*. **105,** 364-375.

Alsheimer, M., Fecher, E. and Benavente, R. (1998). Nuclear envelope remodelling during rat spermiogenesis: distribution and expression pattern of LAP2/thymopoietins. *J. Cell Sci.* **111**, 2227–2234.

Amin, R., Shukla, A., Zhu, J. J., Kim, S., Wang, P., Tian, S. Z., Tran, A. D., Paul, D., Cappell, S. D., Burkett, S., *et al.* (2021). Nuclear pore protein NUP210 depletion suppresses metastasis through heterochromatin-mediated disruption of tumor cell mechanical response. *Nat. Commun.* **12**, 7216.

Arafah, K., Lopez, F., Cazin, C., Kherraf, Z. E., Tassistro, V., Loundou, A., Arnoult, C., Thierry-Mieg, N., Bulet, P., Guichaoua, M. R., *et al.* (2021). Defect in the nuclear pore membrane glycoprotein 210-like gene is associated with extreme uncondensed sperm nuclear chromatin and male infertility: A case report. *Hum. Reprod.* **36**, 693–701.

Calvi, A., Wong, A. S. W., Wright, G., Wong, E. S. M., Loo, T. H., Stewart, C. L. and Burke, B. (2015). SUN4 is essential for nuclear remodeling during mammalian spermiogenesis. *Dev. Biol.* **407**, 321–330.

Chi, Y.-H., Cheng, L. I., Myers, T., Ward, J. M., Williams, E., Su, Q., Faucette, L., Wang, J.-Y. and Jeang, K.-T. (2009). Requirement for *Sun1* in the expression of meiotic reproductive genes and piRNA. *Development* **136**, 965–973.

Cohen, M., Feinstein, N., Wilson, K. L. and Gruenbaum, Y. (2003). Nuclear Pore Protein gp210 Is Essential for Viability in HeLa Cells and Caenorhabditis elegans. *Mol. Biol. Cell* **14**, 4230–4237.

Ding, X., Xu, R., Yu, J., Xu, T., Zhuang, Y. and Han, M. (2007). SUN1 Is Required for Telomere Attachment to Nuclear Envelope and Gametogenesis in Mice. *Dev. Cell* **12**, 863–872.

Dooher, G. B. and Bennett, D. (1973). Fine structural observations on the development of the sperm head in the mouse. *Am J. Anat.* **136**, 339–361.

Elkhatib, R., Longepied, G., Paci, M., Achard, V., Grillo, J.-M., Levy, N., Mitchell, M. J. and Metzler-Guillemain, C. (2015). Nuclear envelope remodelling during human spermiogenesis

involves somatic B-type lamins and a spermatid-specific B3 lamin isoform. *Mol. Hum. Reprod.* **21**, 225–236.

Elkhatib, R. A., Paci, M., Boissier, R., Longepied, G., Auguste, Y., Achard, V., Bourgeois, P., Levy, N., Branger, N., Mitchell, M. J., *et al.* (2017). LEM-domain proteins are lost during human spermiogenesis but BAF and BAF-L persist. *Reproduction* **154**, 387–401.

Gao, Q., Khan, R., Yu, C., Alsheimer, M., Jiang, X., Ma, H. and Shi, Q. (2020). The testis-specific LINC component SUN3 is essential for sperm head shaping during mouse spermiogenesis. *J. Biol. Chem.* **295**, 6289–6298.

Göb, E., Schmitt, J., Benavente, R. and Alsheimer, M. (2010). Mammalian Sperm Head Formation Involves Different Polarization of Two Novel LINC Complexes. *PLoS One* **5**, e12072.

Ho, H.-C. (2010). Redistribution of nuclear pores during formation of the redundant nuclear envelope in mouse spermatids. *J. Anat.* **216**, 525–532.

Huang, C., Gong, H., Mu, B., Lan, X., Yang, C., Tan, J., Liu, W., Zou, Y., Li, L., Feng, B., *et al.* (2022). BAF-L Modulates Histone-to-Protamine Transition during Spermiogenesis. *Int. J. Mol. Sci.* **23**, 1985.

Khan, M., Jabeen, N., Khan, T., Hussain, H. M. J., Ali, A., Khan, R., Jiang, L., Li, T., Tao, Q., Zhang, X., *et al.* (2018). The evolutionarily conserved genes: *Tex37*, *Ccdc73*, *Prss55* and *Nxt2* are dispensable for fertility in mice. *Sci. Rep.* **8**, 4975.

Kierszenbaum, A. L. and Tres, L. L. (2004). The acrosome-acroplaxome-manchette complex and the shaping of the spermatid head. *Arch. Histol. Cytol.* **67**, 271–284.

Lehti, M. S. and Sironen, A. (2016). Formation and function of the manchette and flagellum during spermatogenesis. *Reproduction* **151**, R43–R54.

Lu, Y., Oura, S., Matsumura, T., Oji, A., Sakurai, N., Fujihara, Y., Shimada, K., Miyata, H., Tobita, T., Noda, T., *et al.* (2019). CRISPR/Cas9-mediated genome editing reveals 30 testis-enriched genes dispensable for male fertility in mice. *Biol. Reprod.* **101**, 501–511.

Miyata, H., Castaneda, J. M., Fujihara, Y., Yu, Z., Archambeault, D. R., Isotani, A., Kiyozumi, D., Kriseman, M. L., Mashiko, D., Matsumura, T., *et al.* (2016). Genome engineering uncovers 54 evolutionarily conserved and testis-enriched genes that are not required for male fertility in mice. *Proc. Nat. Acad. Sci. USA* **113**, 7704–7710.

Nagirnaja, L., Lopes, A. M., Charng, W.-L., Miller, B., Stakaitis, R., Golubickaite, I., Stendahl, A., Luan, T., Friedrich, C., Mahyari, E., *et al.* (2022). Diverse monogenic subforms of human spermatogenic failure. *Nat. Commun.* **13**, 7953.

Niu, C.-M., Xia, M.-M., Zhong, Y.-N. and Zheng, Y. (2021). Barrier-To-Autointegration Factor 2 is Not Essential for Spermatogenesis or Fertility. *Cytogenet. Genome Res.* **161**, 167–177.

Paonessa, F., Evans, L. D., Solanki, R., Larrieu, D., Wray, S., Hardy, J., Jackson, S. P. and Livesey, F. J. (2019). Microtubules Deform the Nuclear Membrane and Disrupt Nucleocytoplasmic Transport in Tau-Mediated Frontotemporal Dementia. *Cell Rep.* **26**, 582-593.

Pasch, E., Link, J., Beck, C., Scheuerle, S. and Alsheimer, M. (2015). The LINC complex component Sun4 plays a crucial role in sperm head formation and fertility. *Biol. Open* **4**, 1792–1802.

Pierre, V., Martinez, G., Coutton, C., Delaroche, J., Yassine, S., Novella, C., Pernet-Gallay, K., Hennebicq, S., Ray, P. F. and Arnoult, C. (2012). Absence of Dpy19l2, a new inner nuclear membrane protein, causes globozoospermia in mice by preventing the anchoring of the acrosome to the nucleus. *Development* **139**, 2955–2965.

Raices, M. and D'Angelo, M. A. (2012). Nuclear pore complex composition: a new regulator of tissue-specific and developmental functions. *Nat. Rev. Mol. Cell Biol.* **13**, 687–699.

Russell, L. D., Russell, J. A., MacGregor, G. R. and Meistrich, M. L. (1991). Linkage of manchette microtubules to the nuclear envelope and observations of the role of the manchette in nuclear shaping during spermiogenesis in rodents. *Am. J. Anat.* **192**, 97–120.

Schütz, W., Alsheimer, M., Öllinger, R. and Benavente, R. (2005). Nuclear envelope remodeling during mouse spermiogenesis: Postmeiotic expression and redistribution of germline lamin B3. *Exp. Cell Res.* **307**, 285–291.

Sears, R. M. and Roux, K. J. (2020). Diverse cellular functions of barrier-to-autointegration factor and its roles in disease. *J. Cell Sci.* **133,** jcs246546.

Skoko, D., Li, M., Huang, Y., Mizuuchi, M., Cai, M., Bradley, C. M., Pease, P. J., Xiao, B., Marko, J. F., Craigie, R., *et al.* (2009). Barrier-to-autointegration factor (BAF) condenses DNA by looping. *Proc. Nat. Acad. Sci. USA* **106**, 16610–16615.

Tifft, K. E., Segura-Totten, M., Lee, K. K. and Wilson, K. L. (2006). Barrier-to-autointegration factor-like (BAF-L): A proposed regulator of BAF. *Exp. Cell Res.* **312**, 478–487.

Vester, B., Smith, A., Krohne, G. and Benavente, R. (1993). Presence of a nuclear lamina in pachytene spermatocytes of the rat. *J. Cell Sci.* **104**, 557–563.

Zhang, Y., Li, S., Zeng, C., Huang, G., Zhu, X., Wang, Q., Wang, K., Zhou, Q., Yan, C., Zhang, W., *et al.* (2020). Molecular architecture of the luminal ring of the Xenopus laevis nuclear pore complex. *Cell Res.* **30**, 532–540.

Zheng, R., Ghirlando, R., Lee, M. S., Mizuuchi, K., Krause, M. and Craigie, R. (2000). Barrier-to-autointegration factor (BAF) bridges DNA in a discrete, higher-order nucleoprotein complex. *Proc. Nat. Acad. Sci. USA* **97**, 8997–9002.

Figures

Al Dala Ali_Fig.1

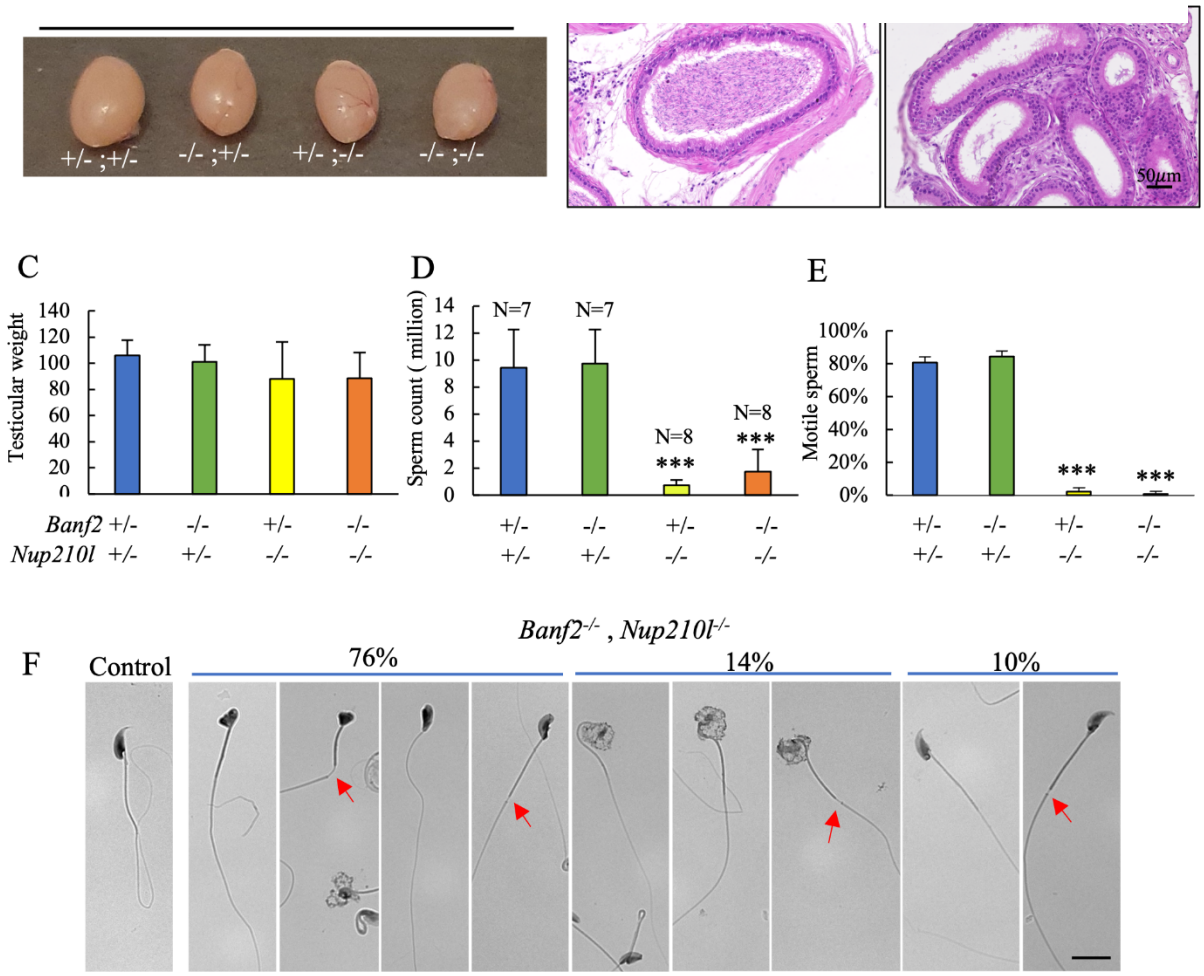

Figure 1: Spermatogenesis disruption in *Banf2,Nup210l* mutant mice

(A) Representative images of adult testes from the indicated genotypes (B) Sections of epididymis stained with hematoxylin and eosin (H&E) from control and *Banf2*$^{-/-}$,*Nup210l*$^{-/-}$ mice (C) The average weight of adult testes in *Banf2*$^{+/-}$,*Nup210l*$^{-/-}$ and *Banf2*$^{-/-}$,*Nup210l*$^{-/-}$ males (n=8) is comparable to the control group (n=7); *p*-value ≥ 0,08 (D) Sperm count was significantly reduced in both *Banf2*$^{+/-}$,*Nup210l*$^{-/-}$ and *Banf2*$^{-/-}$,*Nup210l*$^{-/-}$ while *Banf2*$^{-/-}$,*Nup210l*$^{+/-}$ have normal sperm count. *p*-value < 0.00001, 0.00001 , and 0,82 respectively. (E) Quantification of the number of motile sperm shows that the majority of spermatozoa produced by *Banf2*$^{-/-}$;*Nup210*$^{l-/-}$ and *Banf2*$^{-/-}$;*Nup210l*$^{-/-}$ were immotile (*p*-value <0.00001, 0.00001). (F) Morphological abnormalities of epididymal sperm in both *Banf2*$^{-/-}$,*Nup210*$^{l-/-}$ and *Banf2*$^{-/-}$,*Nup210l*$^{-/-}$ range from abnormal head shape (76%), to a large decondensed sperm head (14%), and only 10% have the usual falciform morphology. Scale bar 10 µm.

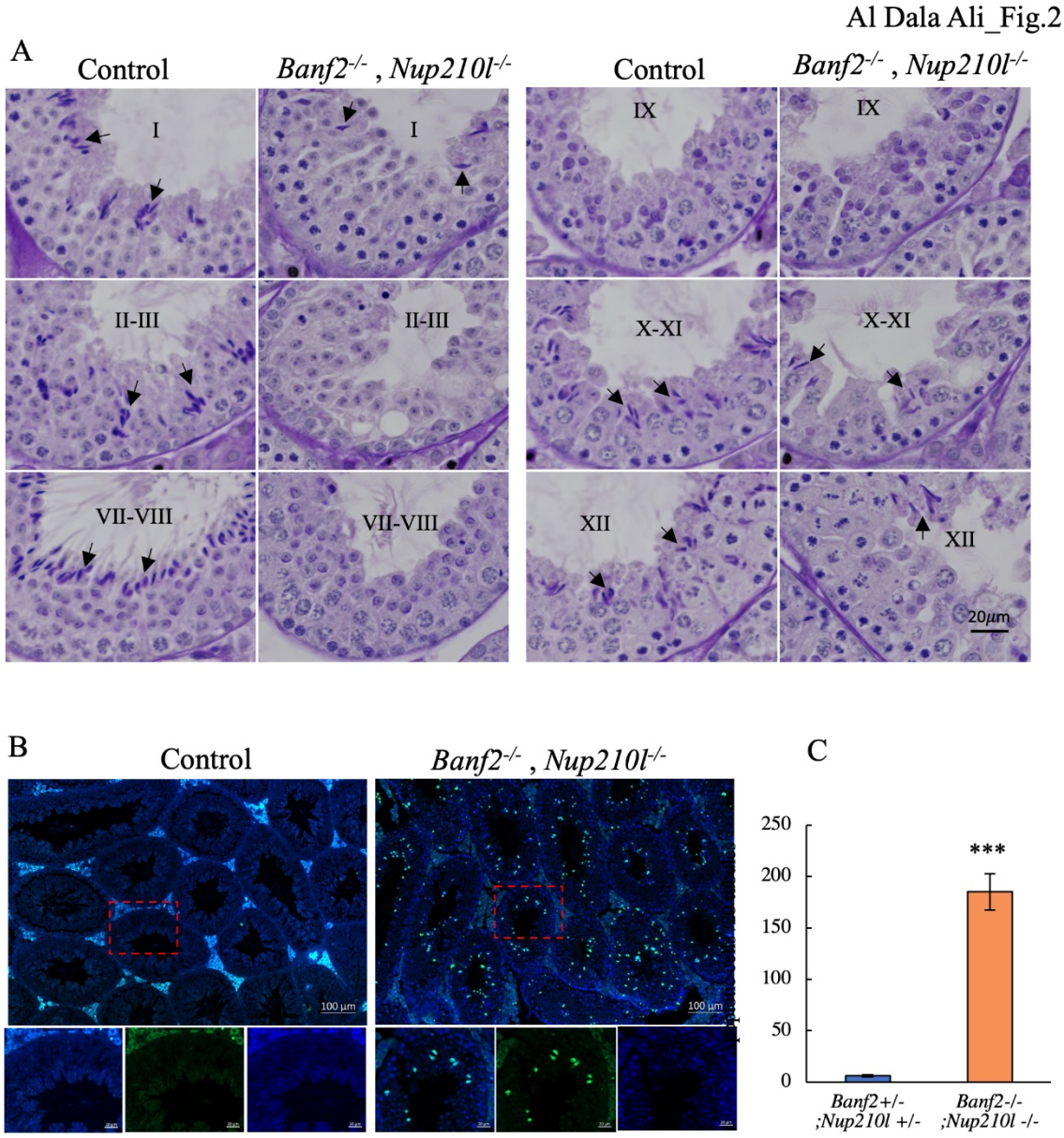

Figure 2: Significant loss of elongated spermatids in *Banf2*$^{-/-}$,*Nup210l*$^{-/-}$ mice

(A) staged comparison of H-PAS-stained *Banf2*$^{-/-}$,*Nup210l*$^{-/-}$ and control littermate testes; Roman numbers represent the stages of the seminiferous tubules. Black arrows mark the elongated spermatid. A noticeable decrease in the number of elongated spermatids is observed in *Banf2*$^{-/-}$,*Nup210l*$^{-/-}$ tubules. (B) Images of TUNEL-stained mouse testis sections, with green indicating TUNEL-positive cells. The number of apoptotic cells has significantly increased in mutant mice. Upon closer examination (magnification of the red boxed area), it is evident that the majority of apoptotic cells are elongated spermatid cells. (C) Quantifications of TUNEL-labeled cells revealed a significant increase in apoptosis in mutant testes. *p*-value = 0.00007.

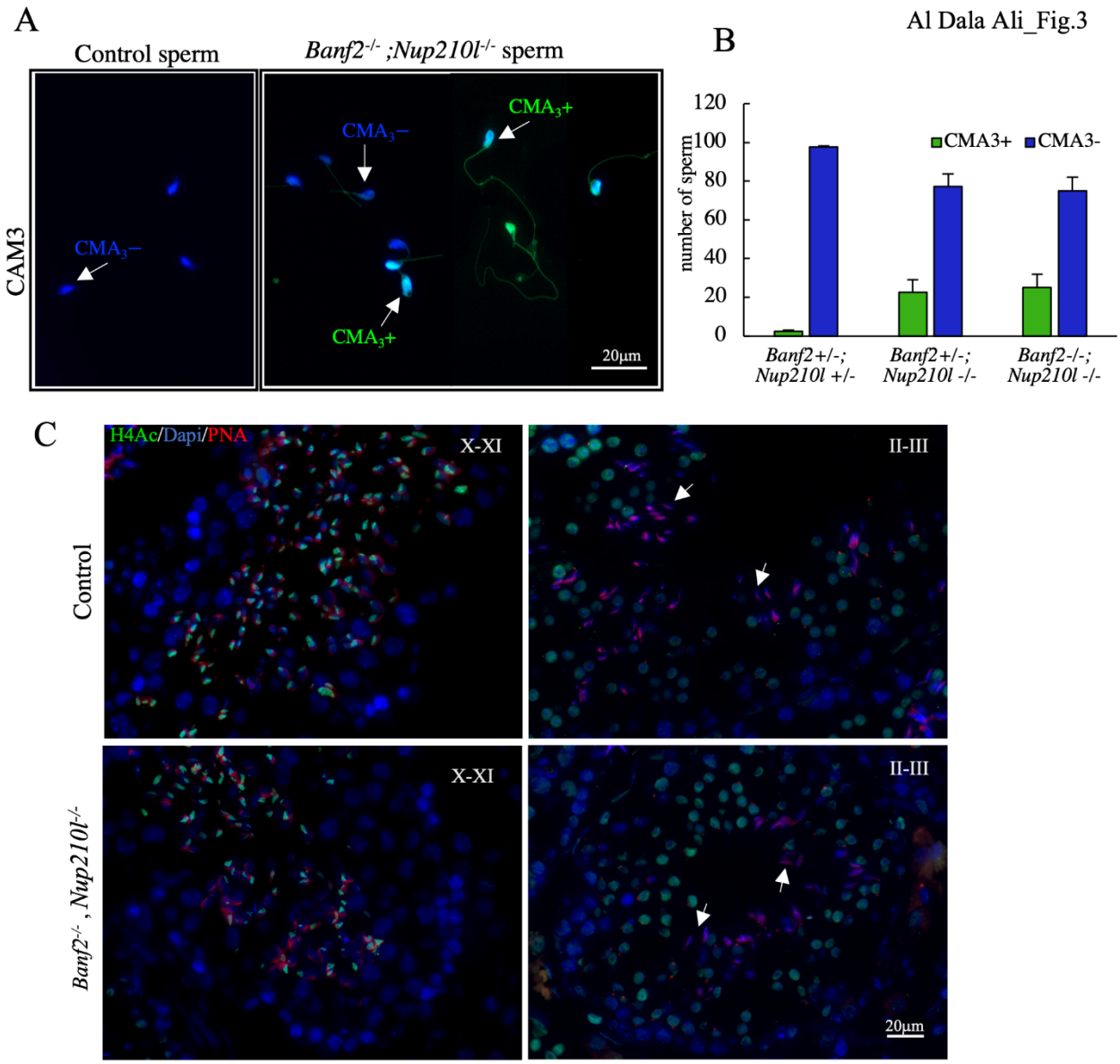

Figure 3: Inefficient histone eviction during spermiogenesis in the *Banf2*$^{-/-}$,*Nup210l*$^{-/-}$

(A) Chromomycin A_3 (CMA_3) was used to stain mouse sperm; CMA_3+ indicates positive spermatozoa (bright green); CMA_3- indicates negative spermatozoa. (B) Quantification of the CMA_3+ and CMA_3- spermatozoa reveals a significant increase in CMA_3+ sperm in the *Banf2*$^{-/-}$,*Nup210l*$^{-/-}$, with a *p*-value= 0.005. (C) Immunoflourescence with antibody specific to acetylated Histone 4 (H4Ac) is performed on testis sections from mutant and control littermates.

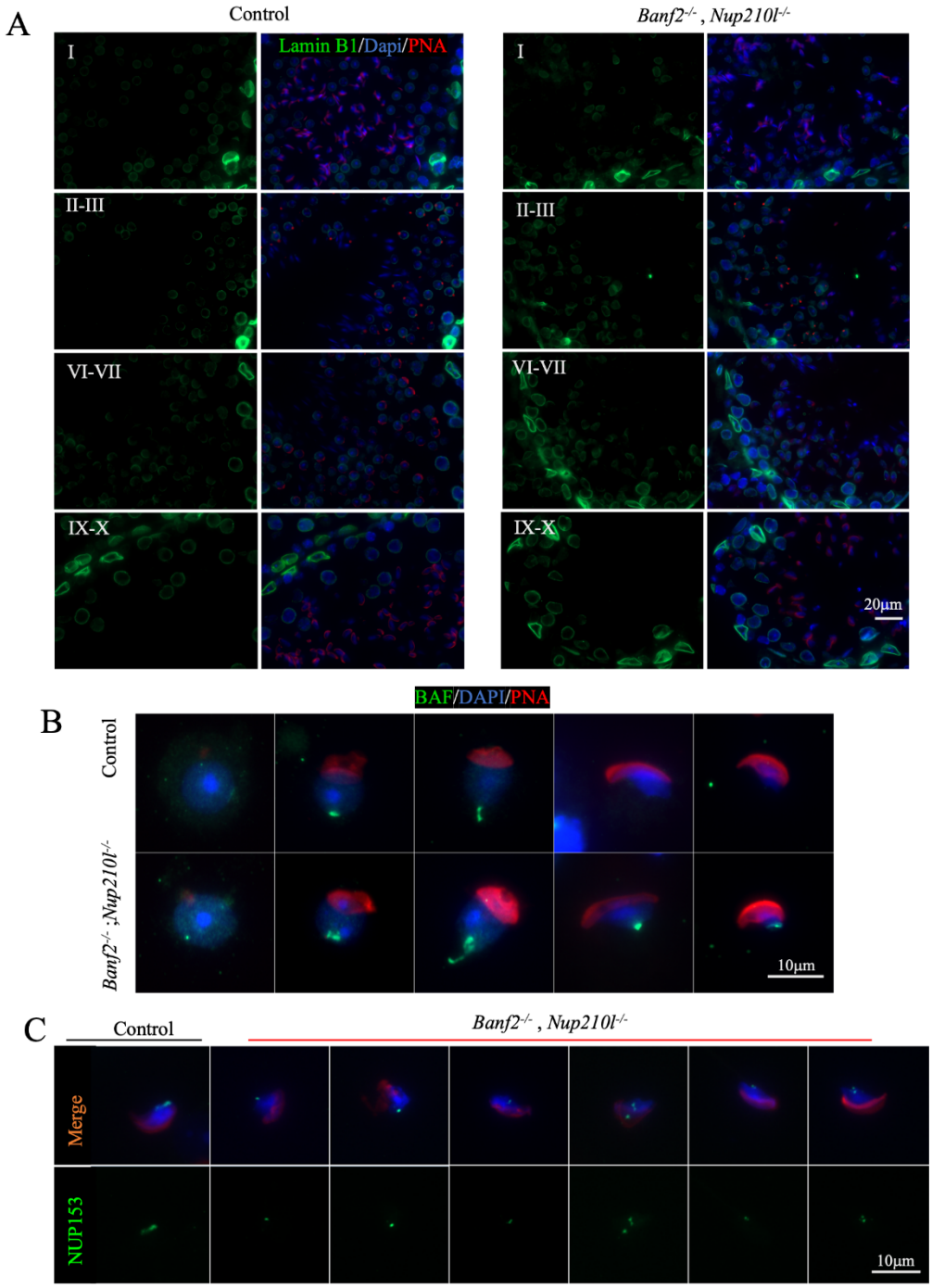

Figure 4: *Banf2*$^{-/-}$*,Nup210l*$^{-/-}$ spermatids exhibit disorganization of NE components. (A) immunofluorescence of testis sections from mutant and control littermates with antibody against Lamin B1 (green), nuclei counterstained with DAPI (blue) and acrosome by PNA (red) as an acrosomal marker to identify the stages of spermatogenesis. (B) Immunofluorescence assessment of BAF localization using a polyclonal antibody against BAF (green), nuclei labeled with DAPI (blue), and acrosome by PNA (red) (C) nuclear pore complex (NPC) localization was detected with a specific antibody against NUP153 (green); nuclei were counterstained with DAPI and acrosomes with PNA.

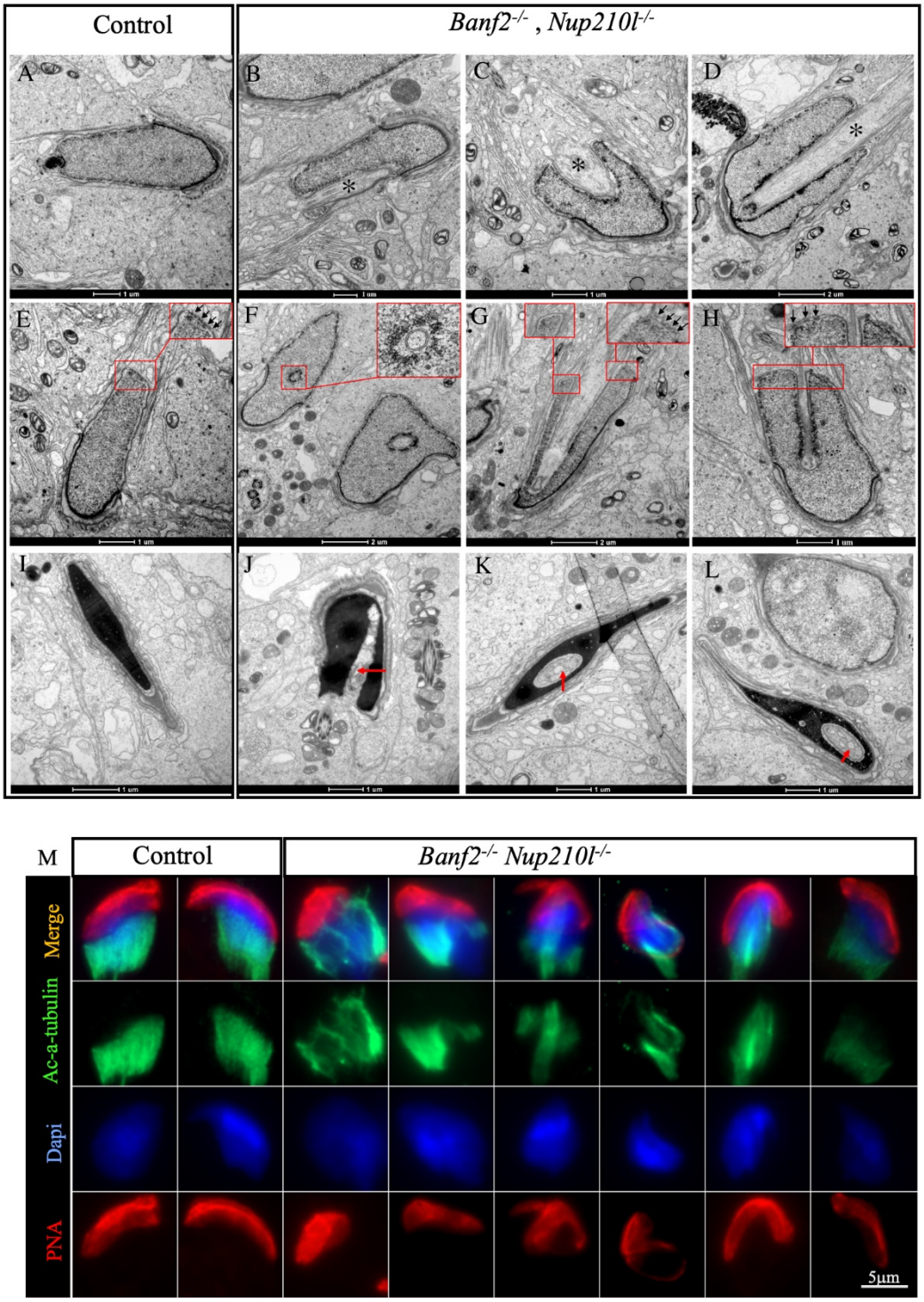

Figure 5: Manchette formation is defective in *Banf2*$^{-/-}$,*Nup210l*$^{-/-}$. Electronic microscopy images of spermatid (step 10–12) from control and mutant mice. As shown by an asterisk (B, C, or D), the *Banf2*$^{-/-}$,*Nup210l*$^{-/-}$ spermatids exhibit nuclear invagination by ectopic microtubules. A transverse section across step 10 spermatid shows that nuclear invagination is composed of microtubular bundles surrounded by a NE (top insert of F). NPC is mostly present on one side of the nuclear invagination, as indicated by the black arrows in the top inserts of (G and H). Step 16 spermatids still have an invagination in the nucleus, the red arrows (J, K, and L) but show that manchette microtubules have depolymerized and been replaced by vacuoles. (M)

Immunofluorescence on disaggregated testes using an antibody against acetylated alpha tubulin (Ac-α-tubulin) shows evident disorganization of manchette microtubules.